Hindawi
Advances in Civil Engineering
Volume 2024, Article ID 8824310, 17 pages
https://doi.org/10.1155/2024/8824310

Research Article

A Wooden Pin Reinforcement of Ancient Chinese Wooden Temple: A Case of Daxiong Hall

Hua Zhang,[1] Wuping Gao ,[2] and Yanling Wang[1]

[1]*Architectural Art Teaching and Research Section, College of Architecture and Art Design, Hebei Academy of Fine Arts, Shijiazhuang 050700, China*
[2]*Tianjin Earthquake Agency, Tianjin 300201, China*

Correspondence should be addressed to Wuping Gao; gwp2023@126.com

Received 21 March 2023; Revised 24 September 2023; Accepted 19 January 2024; Published 28 February 2024

Academic Editor: Giosuè Boscato

Post and lintel frame is a prominent architectural structure in Chinese temple architecture, characterized by its wooden construction. Mortise–tenon joints (MTJs) serve as the primary connection method for these wooden structures, employing straight mortise nodes (SMNs) and through-mortise joints (TMNs). This study presents a method that utilizes wooden pins to reinforce MTJs, enhancing the seismic performance of timber frame structures. Finite element (FE) simulation verifies the effectiveness of wooden pins in reinforcing both SMNs and TMNs, leading to improved load-bearing capacity and ductility of the MTJs. Additionally, the study confirms that reinforced nodes help to restrict the displacement changes within the wooden frame. The paper also investigates the optimal distribution of MTJs reinforced by the wooden pins throughout the structure, with the aim of enhancing the wood frame's seismic performance. The results show the bearing capacity of MJT reinforced with wooden pins is approximately 11.3% higher compared to that of MTJ without reinforcement. The reinforcement of wood pins effectively controls the horizontal displacement of the overall structure of the wooden frame, which is reduced by about 50%–62% compared with the unreinforced wooden frame. The locating the wooden pin-reinforced MTJs in the outer columns and middle layer columns reduces the structural displacement, which is 31.53% in X direction, 5% in Y direction, and 25.86% in Z direction.

1. Introduction

The ancient wooden structure has had a profound impact on the architectural culture of China and Southeast Asia, making it a unique system in the history of world architecture. Mortise–tenon joints (MTJs) are the characteristic construction technique used in traditional wooden structures. These joints allow the wooden components to form an integrated structure capable of meeting various requirements and withstanding different loads [1]. The first usage of MTJs can be traced back to the wooden structures at the Neolithic Hemudu site [2]. However, MTJs are considered weak points in the timber structures [3]. In their study on the damage to the Shuanghe Confucius Temple during the 2019 Changning earthquake, Bai et al. [4] identified lateral residual displacement of the columns and beams as the main seismic damage to wood structures. Similarly, Liu et al. [5] reported damage to wooden structures primarily caused by MTJ failure during the 2008 Wenchuan earthquake and the 2015 Nepal earthquake. The damaged condition of wood structures often reveals deformation and damage to the key force transmission connections provided by MTJs [1]. In severe cases, MTJ damage can even lead to the structural collapse during strong earthquakes [6–8]. Therefore, understanding the mechanical properties of MTJs is crucial for the reinforcement of ancient wooden structures.

At present, the reinforcement materials for MJT are fiber-reinforced polymers [9–13], steel components [14], damper [15, 16], shape memory alloy [17], bolt and screw [18–21], etc. Kim et al. [22] reinforced the MJT with GFRP and FRP. The result shows the bearing capacity of the tensile area of the MJT was significantly improved. The application of steel plate [23], steel strip [24], and angle steel [25] improves the stiffness and energy dissipation capacity of MJT. In terms of the cyclic behavior and energy dissipation of the reinforced MJT, the reinforcement effect of the damper [17] on the MJT is significantly better than that of the other methods. Xie et al. [26] have demonstrated that shape memory alloy can limit the withdrawal of the tenon from the mortise. Tests done by Branco et al. [27] showed that the use of bolts and screws did not increase the in-plane load-bearing capacity (only 1.1 times), and the dissipated energy of the wood-framed walls did not increase. The use of internal bolts (steel bars) to strengthen the connection of timber frame walls is another technique studied by Branco et al. [15]. The influence of the angle of the rod on the bearing capacity in the plane is studied, and the results show that the bearing capacity, stiffness, and dissipated energy are reduced by increasing the angle from 30° to 60°. The above reinforcement method greatly changes the appearance of the MTJs. Strengthening the ancient timber structures should maintain the appearance of the buildings without major changes. This paper proposes a scheme of using wooden pins to reinforce MTJ. This reinforcement method can maintain the original appearance of wood buildings.

For several decades, finite element (FE) simulation has been widely employed by the scholars to study ancient wood structures [28, 29]. Fang et al. [30] developed various numerical modeling strategies to explore the mechanical properties of MTJs in traditional wood structures and deduced the average stiffness range of through-mortise joints (TMNs). Chen et al. [31] demonstrated the mechanical properties of six different MTJs through numerical simulations. Zhao et al. [32] and Dong et al. [33] proposed variable stiffness elements and two nodal space virtual spring elements, respectively, to simulate MTJs. Guan et al. [34] used a three-dimensional FE model to analyze the relationship between bending moment resistance and deformation angle at the node. Wang et al. [35] proposed simplifying MTJs as variable rigid connections and employed three-dimensional dynamic elastoplastic FE analysis to determine the natural frequency and mode shape of Xi'an Dongmen City Tower. Evaluating the overall performance of wood structures based on numerical analysis of MTJ reinforcement becomes crucial in assessing the effectiveness of such reinforcement.

In recent years, FE analysis of wooden structure performance has rapidly advanced. Mathematical models considering skeleton curve characteristics, rotational stiffness degradation laws, failure modes, and energy have been developed. To create an accurate FE model of the Daxiong Hall, the following assumptions were made. According to the Qinggong Ministry's "Code of Engineering Practice" [36] regarding wooden buildings, the walls within the structure do not bear any load. Therefore, the FE model does not consider the impact of the walls on the structure.

The typical beam-lifting wooden structure of Daxiong Hall is selected as the research object. Based on consulting relevant literature such as "Construction French Style" [37], the "Engineering Practice Rules" [36], and "Wooden Construction Technology of Ancient Chinese Buildings" of the Ministry of Qing Engineering [38], the straight mortise node (SMN) and through-mortise node (TMN) are studied. Based on the survey data of Daxiong Hall and the properties of construction materials, this paper carries out a numerical analysis of the SMN and TMN reinforced by wood pins. The reinforcement scheme of SMN and TMN is applied to the timber structures, and numerical analysis is carried out to verify the reinforcement effect. According to the analysis results, the optimization scheme for wood pin reinforcement was obtained.

2. Case Study

2.1. Basic Information of the Daxiong Hall. Xingguo Temple, situated in Lushi County, Henan Province, was originally constructed during the Southern Liang dynasty around 536 AD. The temple comprises various buildings, including the mountain gate, Daxiong Hall, and Tianwang Hall. Over time, Xingguo Temple has undergone several demolitions and reconstructions. The two-story Daxiong Hall of Xingguo Temple exhibits Qing-style architecture (Figure 1(a)). During the investigation of the temple, it was observed that the columns and beams were connected using MTJ (Figure 1(b)). These components were prefabricated in a factory and then assembled on-site. The investigation revealed varying degrees and types of damage in some of the MTJ connections (Figures 1(d) and 1(e)). To reinforce the MTJ, wooden pins were used (Figures 2 and 3). Numerical analysis was conducted on the MTJ to establish the performance of the Yipin framework (Figure 1(c)) and expand the numerical analysis. To adhere to the precise construction requirements of the MTJ, the width of the tenon's opposite top was made "half of the thickness of the column." Wooden pins were used to reinforce the original tenon and tenon nodes, and their placement followed the principles of "Ancient Chinese building wood construction technology" [39]. The wooden pins were located the center position on both sides of the mortising head (Figures 2 and 3).

2.2. Basic Assumptions of the FE Model. To establish the FE model of the Daxiong Hall with maximum possible accuracy, the following assumptions were adopted. According to the Qinggong Ministry's "Code of Engineering Practice" [36] on the relevant requirements for wooden buildings, the effect of the wall on the structure is not considered in the FE model because the walls in the building do not bear the load.

The roof and top surface loads are transmitted to the beams, and finally to the columns through the MTJ [40]. The interaction between the columns and beams is analyzed in the FE model. The connection between the column and the ground foundation is hinged connection. There are 16 pillars in the Daxiong Hall, which is erected on the ground foundation buried at a certain depth in the ground. The foundation only provides the upward support and horizontal friction for the column. There is no corresponding rotational constraint between the columns.

The MTJ connection is considered a nonlinear rotating spring. The connection between the MTJs is simulated using variable stiffness rod elements with rotating springs [41, 42]. Considering the energy dissipation capacity of the MTJ, the nonlinear rotating spring at the beam is used to simulate the MTJ of the semirigid connection [43–46]. Only the deformation under the action of the bending moment is considered without considering the influence of axial force and establishment on the connection deformation.

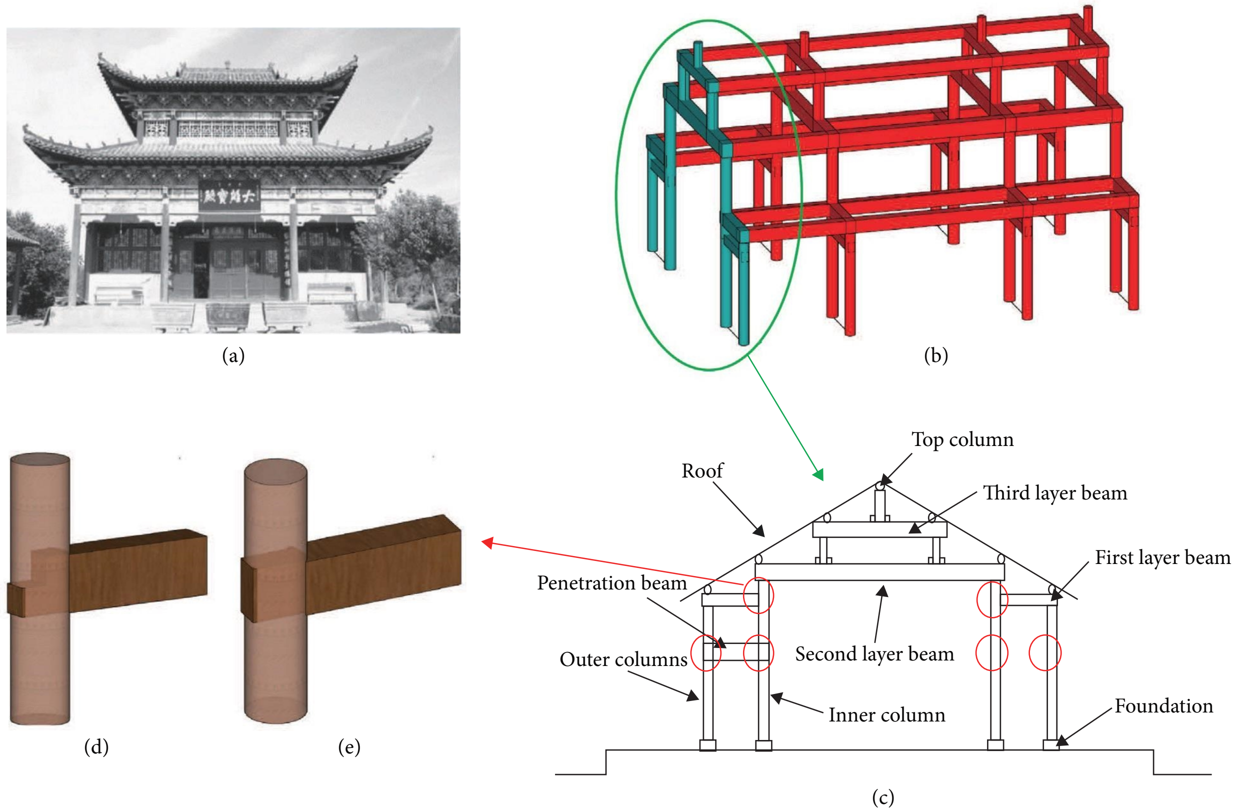

FIGURE 1: Daxiong hall. (a) Photograph of Daxiong hall, (b) wooden frame, (c) illustrative diagram of the wooden structure, (d) semi-mortise node, and (e) straight mortise node.

FIGURE 2: Reinforcement of SMN.

FIGURE 3: Reinforcement of TMN.

2.3. Material Property Assumptions of the FE Model. The wood fibers inside the wood are arranged in the direction of the trunk. Wood has strong resistance in the axial direction of the trunk. Pride Obara [47] applied orthogonal symmetry theory to wood in 1928. As shown in Figure 4, L represents the longitudinal direction of the wood, R represents the radial direction of the wood, and T represents the chordal direction of the wood. TS is transverse section. RF is radial facets. CC is chord cutouts. Wood can be regarded as an orthogonal material.

The wood is considered to be a nondeformable material. The properties of wood are affected by various factors, such

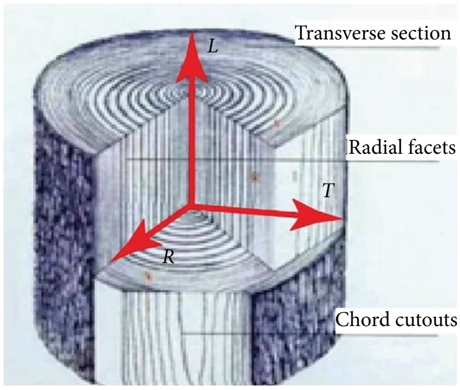

Figure 4: Section plane of wood.

as the type of wood, density, and water content. The occurrence of wood damage or cracks caused by insect erosion, decay, and other reasons influences the mechanical properties of the overall structure. To simplify the calculation, cracking and insect erosion in the wood is not considered for the FE simulation model.

3. FE Simulation Analysis of MTJ

3.1. Constitutive Relations of the Wood

3.1.1. Elastic Constitutive Relations of the Wood. The wood is considered as material elastic symmetry [48]. The performance equation of wood is simplified (Equation (1)).

$$\begin{bmatrix} \sigma_{XX} \\ \sigma_{YY} \\ \sigma_{ZZ} \\ \sigma_{XY} \\ \sigma_{XZ} \\ \sigma_{YZ} \end{bmatrix} = \begin{bmatrix} E_{XXXX} & E_{YYYY} & E_{ZZZZ} & 0 & 0 & 0 \\ E_{XXYY} & E_{YYYY} & E_{YYZZ} & 0 & 0 & 0 \\ E_{XXZZ} & E_{YYZZ} & E_{ZZZZ} & 0 & 0 & 0 \\ 0 & 0 & 0 & E_{XYXY} & 0 & 0 \\ 0 & 0 & 0 & 0 & E_{XZXZ} & 0 \\ 0 & 0 & 0 & 0 & 0 & E_{YZYZ} \end{bmatrix} \begin{bmatrix} \varepsilon_{XX} \\ \varepsilon_{YY} \\ \varepsilon_{ZZ} \\ \varepsilon_{XY} \\ \varepsilon_{XZ} \\ \varepsilon_{YZ} \end{bmatrix}, \tag{1}$$

where σ_{ij} and ε_{ij} are the stress in all directions of the wood and the strain component in the corresponding direction.

The wood of the elastic modulus constant in each direction are calculated (Equations (2) and (3)).

$$\left\{ \begin{array}{c} E_{XXXX} = E_L(1 - \nu_{RT}\nu_{RT})\gamma \\ E_{YYYY} = E_R(1 - \nu_{LT}\nu_{TL})\gamma \\ E_{ZZZZ} = E_T(1 - \nu_{LR}\nu_{RL})\gamma \\ E_{XXYY} = E_L(\nu_{RL} + \nu_{TL}\nu_{RT})\gamma \\ E_{XXZZ} = E_T(\nu_{LT} + \nu_{LR}\nu_{RT})\gamma \\ E_{YYZZ} = E_R(\nu_{TR} + \nu_{LR}\nu_{TL})\gamma \\ E_{XYXY} = 2G_{XY} \\ E_{XZXZ} = 2G_{XZ} \\ E_{YZYZ} = 2G_{YZ} \end{array} \right\}, \tag{2}$$

$$\left\{ \begin{array}{c} \varepsilon_{XY} = \dfrac{\gamma_{LR}}{2} \\ \varepsilon_{XZ} = \dfrac{\gamma_{LT}}{2} \\ \varepsilon_{YZ} = \dfrac{\gamma_{RT}}{2} \\ \gamma = \dfrac{1}{(1 - \nu_{LR}\nu_{RL} - \nu_{RT}\nu_{TR} - \nu_{LT}\nu_{TL} - 2\nu_{RL}\nu_{TR}\nu_{LT})} \end{array} \right\}, \tag{3}$$

where E_L, E_R, and E_T are the modulus of elasticity in the L, R, and T directions of wood, and G_{XY}, G_{XZ}, and G_{YZ} represent the shear modulus of the LR, LT, and RT surface, respectively; ν_{ij} is the Poisson's ratio in the corresponding surface direction.

3.1.2. Plastic Constitutive Relations of the Wood. Most of the FE simulation of wooden components adopts the Hill yield criterion, which can reflect the regional distribution of wood stress. The relevant parameters in the elastic constitutive equation are defined using the properties of each isotropic material orthotropic of wood. The values of each parameter involved are experimentally measured. To accurately express the properties of each orthotropic of wood, herein, the generalized Hill plastic yield criterion is used to simulate the changes in the plastic stage of wood. Under ideal conditions, the wood is considered to be an elastoplastic material (Equations (4) and (5)).

$$\sigma^2 = a_1(\sigma_{22} - \sigma_{33})^2 + a_2(\sigma_{33} - \sigma_{11})^2 + a_3(\sigma_{11} - \sigma_{22})^2 + 2a_4\sigma_{23}^2 + 2a_5\sigma_{13}^2 + 2a_6\sigma_{12}^2, \tag{4}$$

$$\left\{ \begin{array}{c} a_1 = \dfrac{1}{2}\left(\dfrac{1}{R_{22}^2} + \dfrac{1}{R_{33}^2} - \dfrac{1}{R_{11}^2}\right) \\ a_2 = \dfrac{1}{2}\left(\dfrac{1}{R_{11}^2} + \dfrac{1}{R_{33}^2} - \dfrac{1}{R_{22}^2}\right) \\ a_3 = \dfrac{1}{2}\left(\dfrac{1}{R_{11}^2} + \dfrac{1}{R_{22}^2} - \dfrac{1}{R_{33}^2}\right) \\ a_4 = \dfrac{3}{2R_{23}^2} \\ a_5 = \dfrac{3}{2R_{13}^2} \\ a_6 = \dfrac{3}{2R_{12}^2} \end{array} \right\}, \tag{5}$$

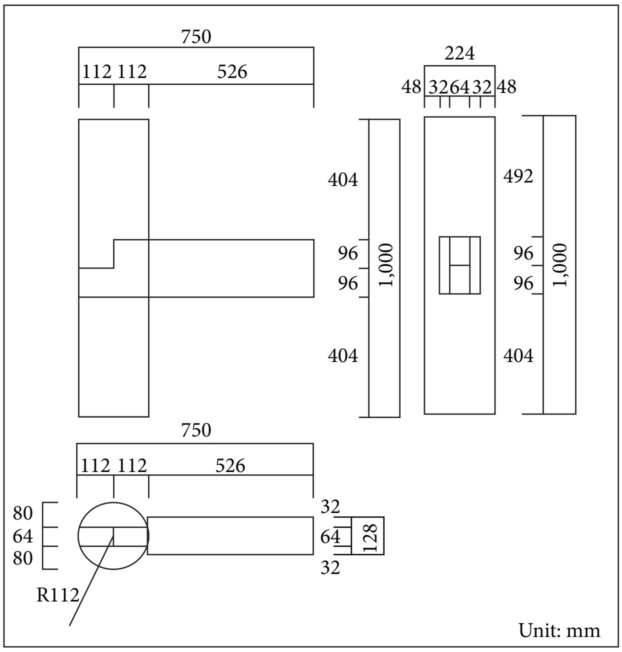

Figure 5: Size of the SMN.

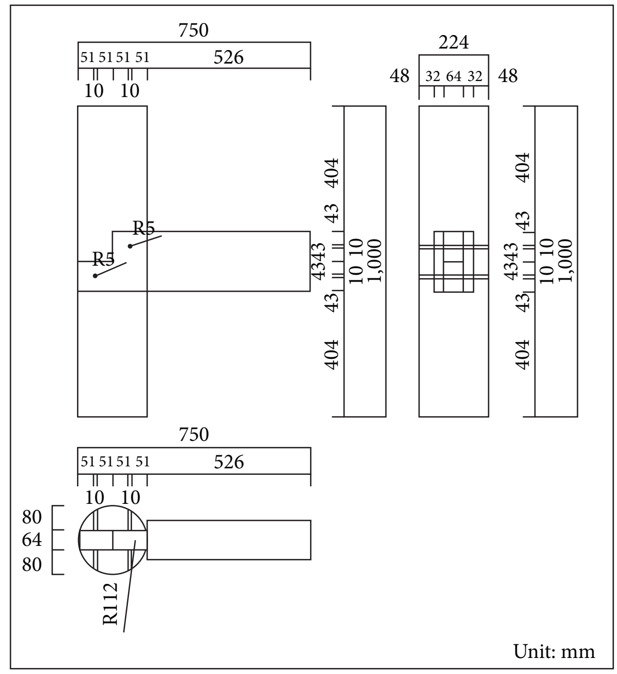

Figure 6: Size of the reinforced SMN.

where σ is the equivalent force. R_{ij} is the strength ratio in the direction of the main axis of the material.

The specific expression for the strength ratio of R_{ij} in the direction of the material spindle is Equation (6).

$$\left\{\begin{aligned} R_{11} &= \frac{f_{11}}{f_0} \\ R_{22} &= \frac{f_{22}}{f_0} \\ R_{33} &= \frac{f_{33}}{f_0} \\ R_{13} &= \frac{\sqrt{3}f_{13}}{f_0} \\ R_{23} &= \frac{\sqrt{3}f_{23}}{f_0} \\ R_{12} &= \frac{\sqrt{3}f_{12}}{f_0} \end{aligned}\right\}, \tag{6}$$

where f_{11}, f_{22}, and f_{33} are the compressive tensile yield strength of wood in the longitudinal, radial, and tangential directions, respectively. f_{12}, f_{13}, and f_{23} are the shear yield strength of wood. The value of f_0 is the same as f_{11}.

3.2. Establishment of FE Model of the MTJ

3.2.1. Geometric Parameters of MJT. The reinforced and unreinforced models of SMNs and TMNs were established by the ABAQUS. The individual parts of the wooden member are modeled separately according to the plane size of the specimen (Figures 5–8).

The FE model dimensions of the SMN and TMN were created based on the dimensions of the test specimen (Table 1).

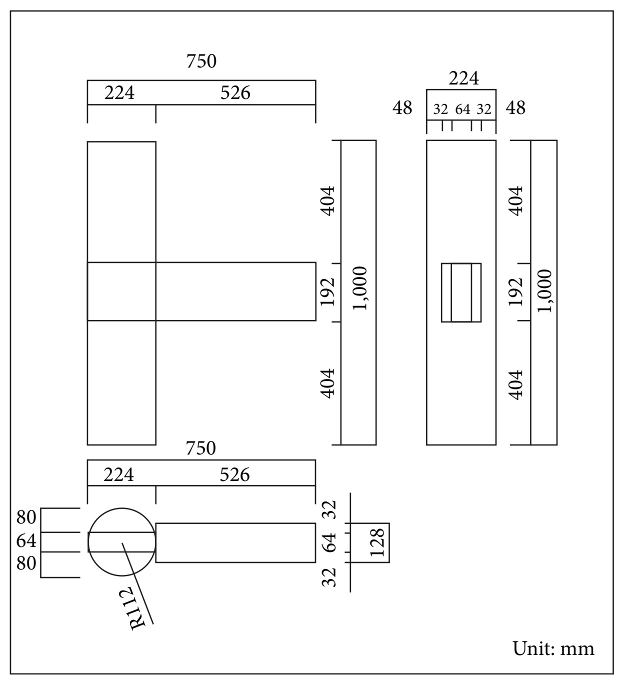

Figure 7: Size of the TMN.

The wooden components such as square, tenon, and post were assembled by the Assembly module of ABAQUS.

3.2.2. Material Property of MJT. The mechanical properties of wood in three directions, axial, radial, and chord, are naturally different. Twenty-one independent elastic parameters involved in orthotropic materials are simplified. Nine elastic values involved in the three directions of the material are defined, which are E_L, E_R, E_T, G_L, G_R, G_T, V_{LR}, V_{LT}, and

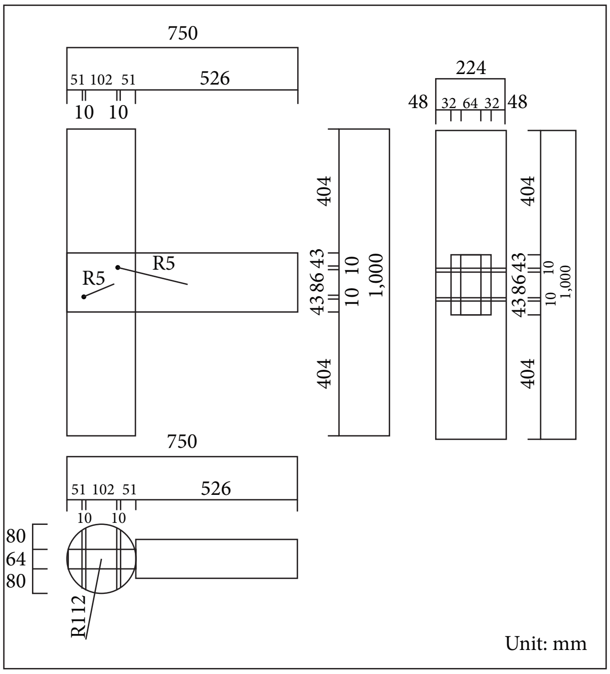

Figure 8: Size of the reinforced TMN.

V_{RT}. E is the modulus of elasticity. G is the shear model. V is the Poisson's ratio. L, R, and T represent the axial, radial, and chordal directions of the wood, respectively.

The material selected for the seismic test of the MTJ model of wooden components is larch, and the mechanical property data of camphor pine used in the simulation are shown in Table 2.

The Hill yield criterion is based on the von Mises criterion by combining the definition of distortion energy to simulate the yield phase of wood. Considering the difference in performance of wood with different orientations, it is more suitable for wood, which is the orthotropic material. This is defined in ABAQUS using the potential function. The input parameter is the yield stress ratio in all directions of the material. Its parameters are calculated as Equation (7):

$$\left\{\begin{array}{l} R_{LL}=\dfrac{\overline{\sigma}_{LL}}{\sigma^0}; R_{RR}=\dfrac{\overline{\sigma}_{RR}}{\sigma^0}; R_{TT}=\dfrac{\overline{\sigma}_{TT}}{\sigma^0} \\ R_{LR}=\dfrac{\overline{\sigma}_{LR}}{\tau^0}; R_{LT}=\dfrac{\overline{\sigma}_{LT}}{\tau^0}; R_{RT}=\dfrac{\overline{\sigma}_{RT}}{\tau^0} \end{array}\right\}, \quad (7)$$

where σ_{ij} is the strength of the wood in the corresponding L, R, and T directions. σ^0 and τ^0 are the yield stress values referenced when plastic is defined. τ^0 should satisfy the following relationship (Equation 8):

$$\tau^0 = \sqrt{3}\sigma^0. \quad (8)$$

In the material assignment stage, wood sections are created by selecting "solid" and "homogenous" materials. The wood is an orthogonal and anisotropic material. It is necessary to set the material direction inside the wood by setting the local cylindrical coordinate system (Figure 9).

3.2.3. Loading Setup of the FE Model. The loading process includes two steps: (1) The boundary conditions are applied to both ends of the wooden column to control. (2) The displacement control is applied to the loading point. The length of time is set to 1 by the loading situation. The parameters such as the maximum number of incremental steps required in the simulation need to be set according to the actual test situation of the wooden component. Other parameters are set by default. Simultaneously, the facility outputs data, such as components, stress, strain, and displacement contact for postprocessing and analysis.

The connection between the wooden pin and the MTJ adopts mutual contact connection. The outer surface of the wooden pin is defined as the main surface. The inner surface of the wooden pin connection reserved by the mortise and the tenon is defined as the secondary surface. The main parameters considered are tangential behavior and normal behavior. For tangential contact, the contact and sliding friction behavior between the wood is usually simulated by using a penalty function, with the friction coefficient set to 0.4. For tangential contact, the Penalty function is usually used to simulate the contact and sliding friction behavior between the wood, and the coefficient of friction is set to 0.4. The normal contact is set as hard contact, which does not allow penetration between the contact surfaces. When the pressure between the contact surfaces is 0 or negative, it is determined that the two contact surfaces are in contact with each other. When the pressure between the contact surfaces is 0 or negative, it is determined that the separation between the two contact surfaces occurs. It is also consistent with the fact that the mortise and tenon node will be dislodged when the actual loading is too large.

The FE simulation situation is consistent with the state of the experiment, the end of the column is completely fixed. The other end is hinged boundary adjustment setting. The line displacement and angular displacement in the X, Y, and Z directions are constrained at one end of the column. The line displacement is constrained at the other end.

3.2.4. Model Mesh Segmentation. The FE model is meshed according to the structural characteristics to guarantee the accuracy of the calculation. Different grid cells have different calculation accuracy and speed. Therefore, considering the time needed for calculation and the accuracy of calculation, this paper uses C3D8R cells for the wooden components involved in the FE simulation, such as wooden beam, wooden column, mortise and tenon, pin. There are two reasons for choosing the C3D8R unit. The first reason is that can ensure the accuracy of the results in the FE simulation, and maximize the calculation of the required displacement results. The second reason is that the distortion deformation occurs locally due to the extrusion and the shear self-locking phenomenon will not occur.

The geometric of the wooden square, wooden columns, and other major wooden components are divided before meshing the model for ensuring the accuracy of mesh

Table 1: The dimensions of the finite element models.

Type of wood	Specimen form	Ratio	Column size (mm)		Beam size (mm)			Tenon size (mm)				Size of wood pin (mm)	
			Length	Caliber	Length	High	Wide	Length	Bigger-high	Less-high	Wide	Caliber	Length
Larch timber	TMN	1 : 3	1,000	224	750	192	128	75	192	96	64	10	220
	SMN							224	192			10	220

Table 2: Performance parameters of *Pinus sylvestris* [49].

E_L (MPa)	E_R (MPa)	E_T (MPa)	μ_{LR}	μ_{LT}	μ_{RT}	G_{LR} (MPa)	G_{LT} (MPa)	G_{RT} (MPa)
14,190	710	710	0.522	0.483	0.522	710	38	710

E_L, elastic modulus of the wood grain; E_R, radial modulus of elasticity of the wood shear grain; E_T, modulus of elasticity of the wood striated chord; μ_{ij}, Poisson's ratio; G_{ij}, shear modulus; *LR*, diameter facet of the wood; *LT*, wood chord facet; *RT*, cross-section of wood.

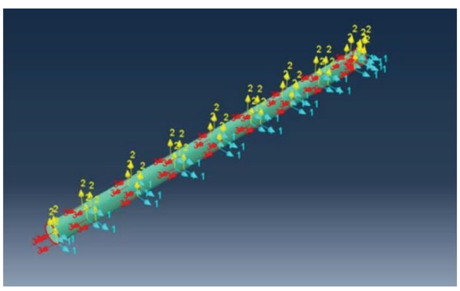

Figure 9: Material assignment direction.

division. Considering, the different areas of the wooden square, wooden columns, mortise and tenon, pin used the different sizes of the mesh for increasing the accuracy of the FE simulation and decline the time required for the calculation By numbers of debugging and calculations, the final determination of the grid size of the wooden column is set to 25 mm (Figure 10(c)); the grid size of the wooden square is set to 30 mm (Figure 10(b)); mortise and tenon as the focus of the calculation, the grid size is set to 20 mm; part of the wooden components mesh division is shown in Figure 10.

3.3. Results and Discussion

3.3.1. The Deformation of the MTJ. The areas with the greatest stress of the MTJ occurs at the junction of mortise and tenon (Figures 11 and 12). The stress distribution is consistent with the typical failure modes of the MTJ. The stress concentration phenomenon of the column occurs in the part, where the tenon is extruded by the upward displacement on the column. The stress concentration of the beam now appears in the part where the mortise is extruded. However, most of the area of the beam and column is in the elastic working state.

The maximum axial tensile stress of the beam and column exceeded the yield strength of the wood, indicating that plastic failure occurred in the key area of the MTJ. The certain detachment has occurred between the mortise and the mouth. The stress of unreinforced SMN on the mortise and mortise joints is significantly greater than that of unreinforced TMN.

Figures 13 and 14 show the deformation of the MTJs in a low-cycle reciprocating load test on the MTJ model [50]. Comparing experimental phenomenon, the stress and deformation of the numerical analysis are close to the typical failure mode of the MTJ in practice. It is consistent with the theoretical analysis that indicate the FE model of the MTJ is reasonable.

The stress of the reinforced MTJ is greater than that of the unreinforced MTJ. Compared to other places, the stress at the wooden pin is larger (Figures 15 and 16). MTJ was reinforced by wood pins and did not produce large cracks. The stress of TMN reinforced by wooden pins is stronger than the SMN reinforced. The reinforcement of the wooden pin reduces the deformation of the MTJ. The effect of wooden pins on SMN is better than that of TMN. The wooden pin will be broken in the actual loading. However, the FE simulation cannot be accurately the crack of the wooden pin.

3.3.2. The Skeleton Curve of the MTJ. The skeleton curve obtained through FE simulation is compared (Figure 17). The skeleton curve of unreinforced specimens obtained through FE simulation is in agreement with the experiment [50]. Integrated the comparison of typical failure modes in 3.3.1, the FE model is reasonable.

The bending moment of the unreinforced TMN gradually flattens when the rotation angle reaches ± 0.05 rad and decreases slightly when the angle reaches -0.12 rad. The bending moment of the reinforced MTJ is larger than the unreinforced MTJ. The bending moment of the unreinforced SMN are larger than TMN. Compared to the other three types of MTJ, the reinforced SMN has the largest bending moment.

4. FE Simulation of the Timber Frame

4.1. The Simplify FE Model of the Timber Frame. MTJ is considered to the semi-rigid characteristic. The bending moment, axial force, and torque of the timber frame can be transmitted via the MTJ. The deformation of MTJ under

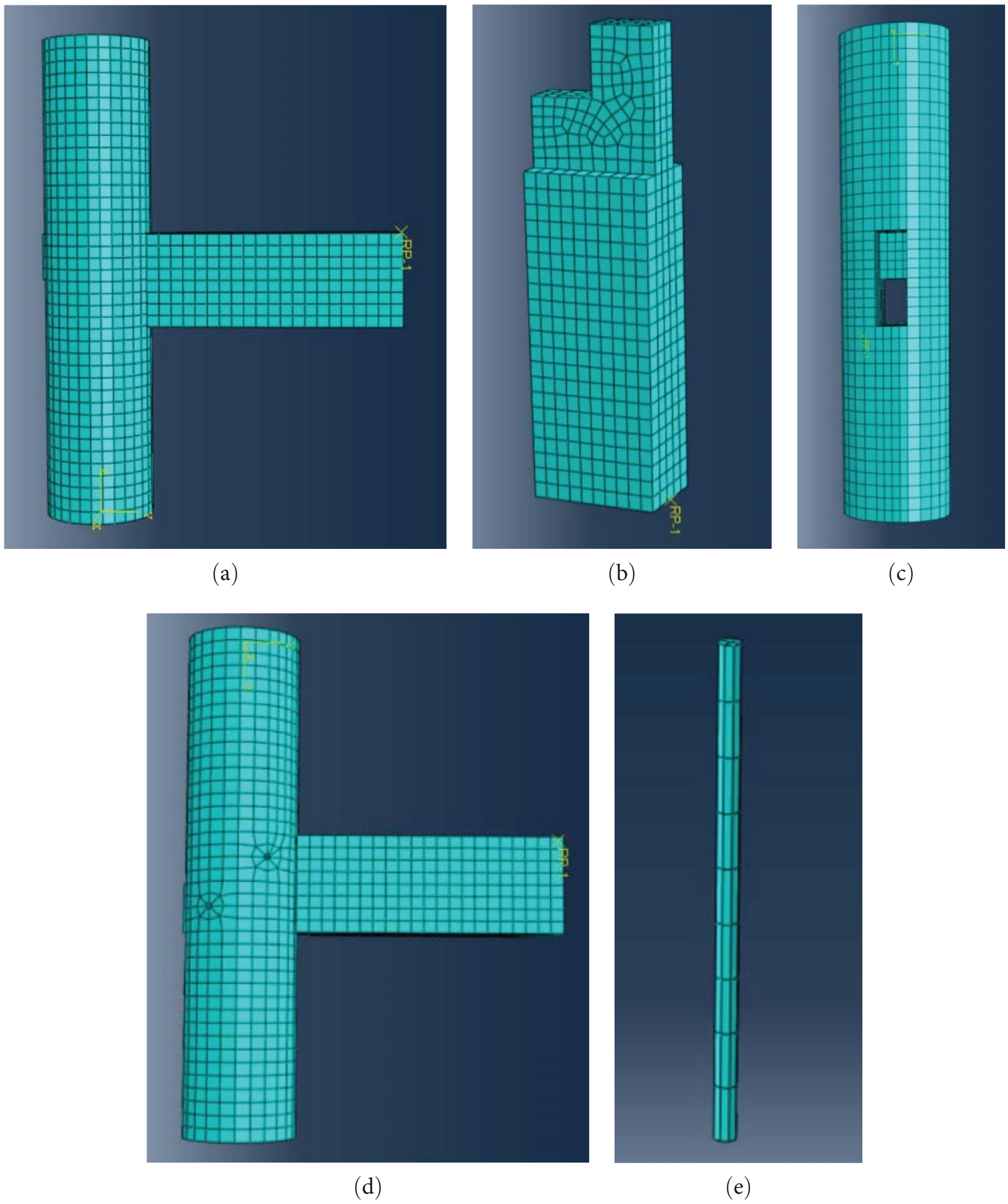

Figure 10: The mashing of the FE models. (a) SMN and TMN without wood pins, (b) beam, (c) column, (d) SMN and TMN with wood pins, and (e) wood pins.

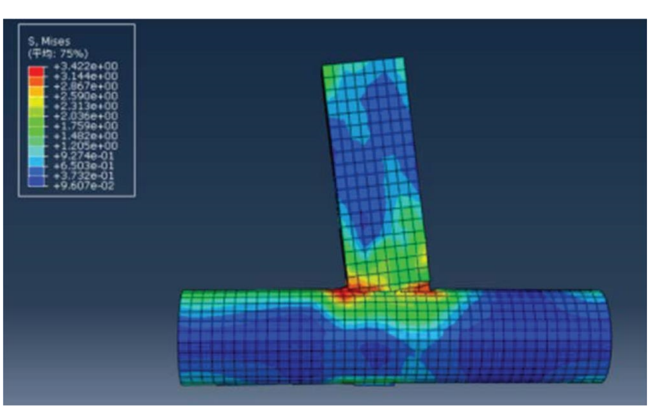

Figure 11: The stress cloud of unreinforced TMN.

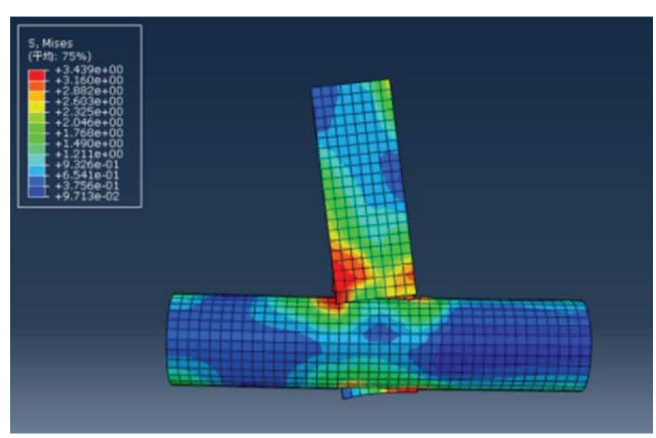

Figure 12: The stress cloud of unreinforced SMN.

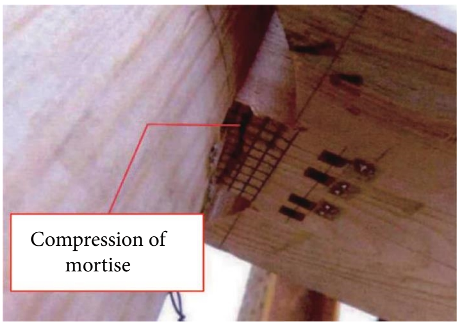

Figure 13: Deformation of the lower surface of the tenon.

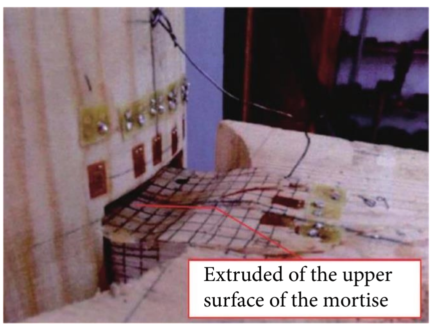

Figure 14: Deformation of the upper surface of the tenon.

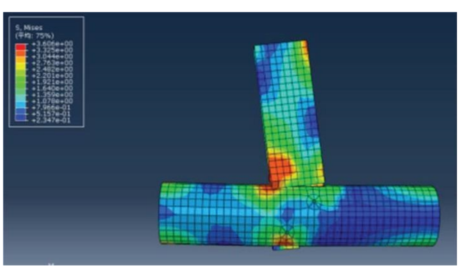

Figure 15: The stress cloud of reinforced TMN.

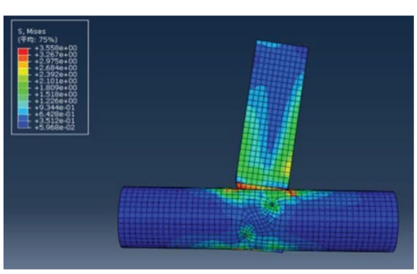

Figure 16: The stress cloud of reinforced SMN.

the action of bending moment is much larger than that produced by axial force, shear force, and torque. The influence of the rotational deformation on the structure is concerned. The mechanical properties of the MTJ are described by the bending moment-angle curve [51]. Therefore, the mechanical properties of the single wooden truss are simulated to reflect the mechanical properties of the post and lintel frame

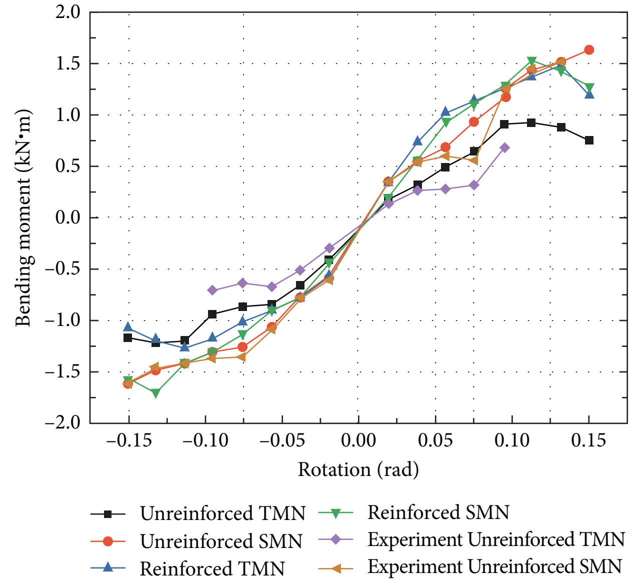

Figure 17: Skeleton curve.

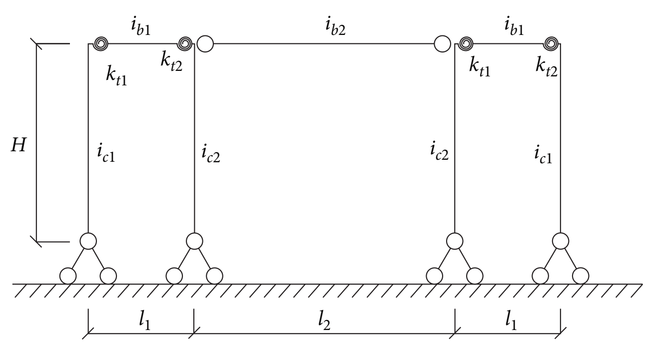

Figure 18: Simplifying the force model.

wooden structure in the FE simulation. The structure of the Daxiong Hall is simplified to the force model (Figure 18).

In the investigation of the Daxiong Hall, the Daxiong Hall is 17 m long and 10 m wide, which is composed of four wooden trusses connected by MTJ. The hall uses camphor pine as the building material. Referring to the practice of the wooden frame in the "Ying zao Fa shi Construction Method" [37] and the Qinggong Ministry "Code of Engineering Practice" [36], the size of the single wooden truss is shown in Table 3.

4.2. Modes of the Timber Frame

4.2.1. The Theory of Model Analysis. Vibration mode is the intrinsic, integral property of structures. Modes refer to the intrinsic vibration characteristics of the mechanical structures, each of which has a specific natural frequency, damping ratio, and modal shape. The main modal characteristics of the structure in a certain vulnerable frequency range by modal analysis method. The actual vibration response of the wooden frame under the action of various external or internal vibration sources can be predicted. The natural frequency and damping ratio information cover can be obtained through

Table 3: Size chart of the single wooden frame.

Column	Outer column	Inner column	Middle layer column	Top column
Diameter (mm)	270	300	300	230
Length (mm)	3,000	5,000	1,500	1,000
Beam	First layer beam	Penetration beam	Second layer beam	Third layer beam
Length (mm)	1,500	1,680	5,300	2,700
Width (mm)	300	190	340	300
Height (mm)	360	270	410	320

modal analysis. The vibration performance of the wooden frame can be obtained. The general dynamic differential equation of motion for multi-degree-of-freedom architectures is shown in Equation (9):

$$\left\{\begin{array}{c}[M]x(t)+[C]x(t)+[K]x(t)=F(t)\\ x=\{x_1\ x_2\ \cdots x_N{}^T\\ F(t)=\{f_1 f_2\ \cdots f_N{}^T\end{array}\right\}, \tag{9}$$

where $[M]$ is the mass matrix; $[C]$ is the damping matrix; $[K]$ is the structural stiffness matrix; $x(t)$ is the displacement vector; $F(t)$ is the load vector of the structure under external action.

The damping of the wood is small. If the external load is not considered, the damping matrix of the structure and the load vector can be omitted from Equation (9). The equation of free vibration motion of the structural system in the assumed undamped Equation (10) is obtained as follows:

$$[M]\ \ddot{x}(t)+[K]x(t)=0. \tag{10}$$

Assuming that the free vibration in the multi-degree-of-freedom system is a simple harmonic motion. The equation can be rewritten as Equation (11):

$$x(t)=\{X\}(t)\sin(\omega t+\theta), \tag{11}$$

where $\{X\}$ is the change in the amplitude of the system, ω is the self-resonating circumferential frequency of the structure, and θ is the phase angle corresponding to the structure.

Substituting Equation (11) into Equation (10) yields Equation (12):

$$-\omega^2[M]\{X\}\sin(\omega t+\theta)+[K]\{X\}\sin(\omega t+\theta)=0. \tag{12}$$

Then, the above equation can be rewritten as Equation (13):

$$[[K]-\omega^2[M]\{X\}]\sin(\omega t+\theta)=0. \tag{13}$$

Considering the amplitude vector $\{X\}\neq 0$ of the structural system, the prerequisite for a nonzero solution of the Equation (14) is given as follows:

$$[K]-\omega_{\mathrm{i}}{}^2[M]=0, \tag{14}$$

where ω_i^2 is the eigenvalue, the range of i is from 1 to the number of degrees of freedom; x_i is the eigenvector; ω_i is the square root of the eigenvalue, which can be obtained that the natural frequency of the structure at the corresponding degrees of freedom $f_i=\omega_i/2\pi$;

4.2.2. The Result and Discussion of Model Analysis. To calculate the 10 mode shape of the wooden frame, this paper mainly uses the Block Lanczos method. The frequency period and participation quality of the structure are analyzed. U_x, U_y, and U_z mark the degree of freedom participation coefficient of the structure in the three translational directions of X, Y, and Z.

It can be seen from that the self-vibration period of the single wooden truss without wood pin is about 1.65 s (Tables 4 and 5). The long-term vibration characteristics of the wood structure is 3.6 times of the site that is 0.45 s, which can effectively avoid the resonance of the wooden structure in the earthquake. The frequency change is large at the 4th and 5th steps, which indicating the 5th mode shape is easier to be excited under the action of the earthquake. The self-vibration period of the wooden truss reinforced by the wood pin is 1.62 s, which is 3.6 times the excellent cycle of the site. Its change is also mainly in the 4th and 5th order.

For the first mode shape, the quality U_x of the structural mode shapes (Figures 19(a) and 20(a)) is much larger than that of U_y and U_z, indicating that the structure has the largest degree of translational freedom in the X direction. The longitudinal stiffness of the surface structure of the first mode shape is the weakest. The overall ability of the structure to cope with longitudinal earthquakes is the worst.

For the second mode shape, the quality U_x and U_z of the structural mode shapes (Figures 19(b) and 20(b)) is close to 0. The value of U_y is 0.2. The translational freedom of the structure in Y direction is the largest, which indicates that the second mode shape is based on horizontal vibration in the Y direction. The lateral stiffness of the structure is greater than the longitudinal lateral stiffness. This is because the structure has a tighter arrangement of components in the transverse aspect and a larger span.

For the third mode shape, the quality U_y and U_z of the structural mode shapes (Figures 19(c) and 20(c)) is close to 0. The U_x is 1.45, which indicates the main vibration type of the structure in X direction of the third mode shape. The period is 0.28 compared to the basic period ($T_3/T_1=0.28$), which

Table 4: Participation coefficients of different degrees of freedom of structures without wood pin.

Mode	Frequency (Hz)	Period(s)	U_x (mm)	U_y (mm)	U_z (mm)
1	0.6028	1.6590	2.0224	−0.0004	0.0001
2	1.9482	0.5133	0.0053	0.0230	−0.0001
3	2.1245	0.4707	−1.4542	−0.0140	0.0016
4	2.3470	0.4261	−0.0026	1.2544	0.0002
5	6.3182	0.1583	0.7013	0.0012	0.0008
6	6.8223	0.1466	0.0063	0.0196	0.1270
7	6.8599	0.1458	0.0005	0.0388	0.0017
8	7.0330	0.1422	−0.0010	0.6115	−0.0042
9	9.1690	0.1091	−0.0006	0.0000	1.2759
10	9.8617	0.1014	0.0015	0.1784	0.0022

Table 5: Participation coefficients of different degrees of freedom of structures with wood pins.

Mode	Frequency (Hz)	Period(s)	U_x (mm)	U_y (mm)	U_z (mm)
1	0.614	1.6298	2.0177	−0.0002	0.0002
2	1.980	0.5050	0.0085	−0.0225	0.0001
3	2.153	0.4644	−1.4500	0.0126	0.0004
4	2.365	0.4228	0.0028	1.2569	0.0002
5	6.349	0.1575	0.7169	−0.0002	−0.0004
6	6.842	0.1462	0.0269	0.0129	0.0041
7	6.897	0.1450	0.0003	0.0361	0.1328
8	7.060	0.1416	−0.0010	0.6212	−0.0088
9	9.189	0.1088	0.0000	0.0005	1.2752
10	9.888	0.1011	0.0014	0.1737	0.0056

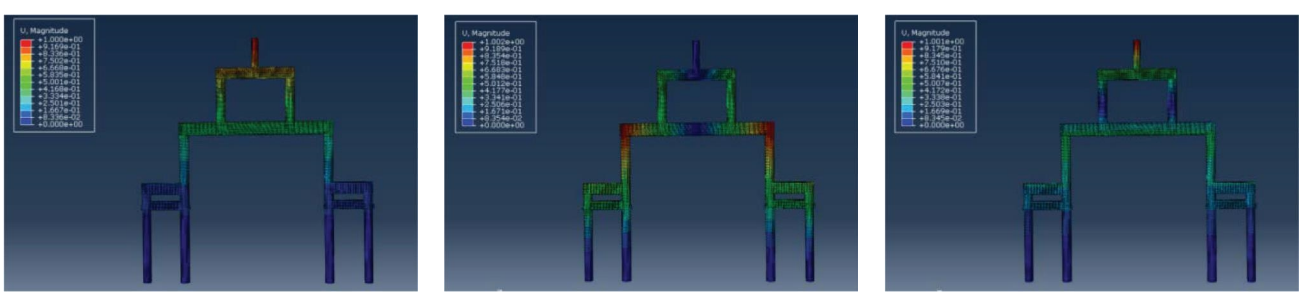

(a) (b) (c)

Figure 19: The three-order mode shape of the single wooden truss wood truss without reinforced. (a) First-order bending mode, (b) second-order bending mode, and (c) third-order bending mode.

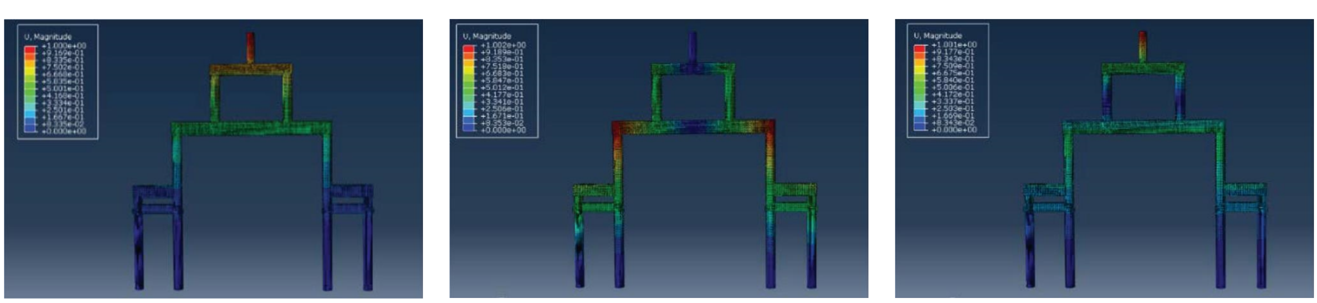

(a) (b) (c)

Figure 20: The three-order mode shape of the single wooden truss wood truss with reinforced. (a) First-order bending mode, (b) second-order bending mode, and (c) third-order bending mode.

Table 6: Seismic acceleration spectral values.

Frequency (HZ)	0.17	0.20	0.25	0.33	0.48	0.58	0.75	1.03	1.32	1.61	2.22	10
Acceleration (m/s^2)	0.063	0.071	0.078	0.086	0.098	0.117	0.147	0.196	0.245	0.294	0.392	0.392

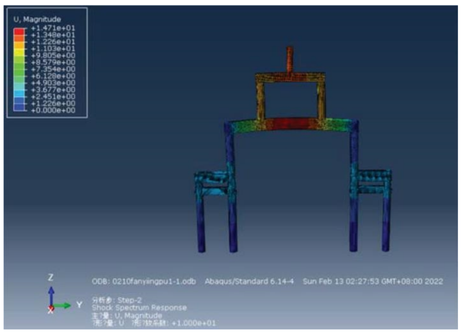

Figure 21: Unreinforced member under response spectrum.

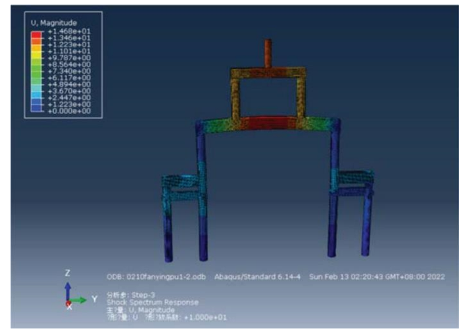

Figure 22: Reinforcement members under the response spectrum.

meets the requirements of the specification that the cycle ratio is less than 0.9, which indicates that the structural layout is relatively reasonable.

The structural properties, vibration types, and modal participation quality of the wood truss reinforced by wood pins are like the wooden truss without wood pin reinforcement. The frequency of the wooden truss is increased after reinforcement that is about 3%. Moreover, the wooden truss reinforced has changed in the 4th-order mode shape compared with the single wooden truss without reinforcement, which shows the reinforcement of wooden pins can significantly reduce the probability of deformation of the structure and reduces the adverse impact of earthquakes on the structure and increase the stiffness of the structure to a certain extent.

4.3. Seismic Response of Timber Frame

4.3.1. Selection of Seismic Response Spectra. The response spectrum analysis is the analysis method based on the modal analysis for calculating the deformation and internal forces. Spectral analysis is calculated by the modal superposition method. The displacements and stresses of the model in conjunction with acceleration, velocity, or displacement response spectra are calculated. According to the Chinese seismic design code [52], the area analyzed is seismic fortification intensity of 6°. The basic seismic acceleration value is 0.05 g. The site category is Class II. The site characteristic period is 0.40 s. The final seismic acceleration spectrum is shown in Table 6.

4.3.2. Response Spectrum Analysis and Results. The acceleration response spectrum is applied in the direction of positive loading. The result is shown in Figures 21 and 22. The maximum displacement of the timber frame without wood pins is 14.71 mm. The maximum displacement of the timber frame with wood pins is 14.68 mm. The larger displacement of the structure is concentrated on the second-layer beams and third-layer beams. Moreover, the lateral displacement of the MJT with wood pins are smaller than the MJT without wood pins. The result indicates the MTJ reinforced by the wooden pins that located on the upper layer of the structure has the better reinforcement effect on the timber frame.

4.4. Dynamical Time-Course Analysis of the Timber Frame

4.4.1. Selection of the Earthquake Wave. This study refer to the requirements of "Code for Seismic Design of Buildings" (GB50011-2010) for the selection of seismic waves for fully estimate and simulate the maximum response of the structure under the action of the earthquake. The result show influence curve on the structure should be statistically consistent with the response spectrum curve. The average impact curve under the action of each seismic wave in the elastic range should not be greater than 20% compared with the response spectrum analysis impact curve. Combined with the seismic fortification intensity of buildings in the region and related parameters, the selected natural seismic waves are shown in Table 7. The artificial waves are randomly generated by Yingjianke software according to the regional conditions (Figures 23 and 24).

4.4.2. Displacement Response of the Timber Frame. The reaction characteristics of the post and lintel frame wooden structure with MTJ as the main connection mode under the action of seismic waves were studied. The seismic waves applied to the wooden structure are simulated. The displacement response of the structure under the action of seismic waves is studied to evaluate the seismic performance. Seismic waves are applied to the single wooden truss from the bottom of the column base in the X direction, Y direction, and bidirectional horizontal direction combined by 1 (horizontal X direction) and 0.85 (horizontal Y direction). The results are listed in Tables 8–10. The response results of the structure to seismic waves are related to the selected seismic waves and the duration of seismic waves. Therefore, the seismic response analysis of the structure can be considered to be 5–10 times the duration of the period of the structure.

To facilitate the comparative analysis, the maximum displacements of the eaves column, lower gold column, upper

Table 7: Seismic waves.

Name	Year	Seismic recording station	Magnitude	Vs (m/s)
Parkfield	1966	Cholame—Shandon Array #12	6.19	408.93
Borrego Mtn	1968	San Onofre—So Cal Edison	6.63	442.88

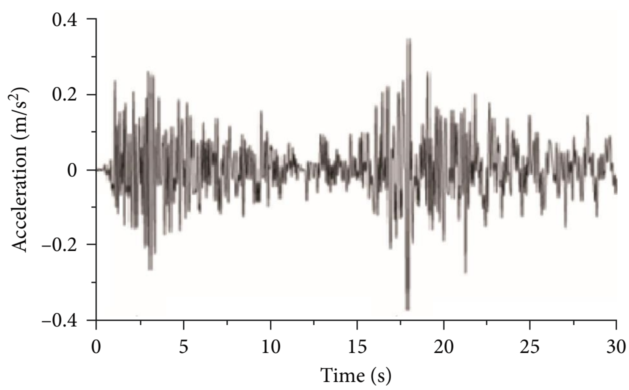

Figure 23: Parkfield seismic wave.

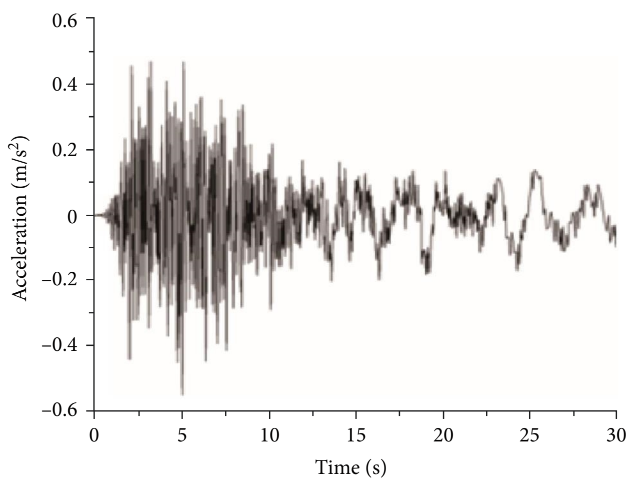

Figure 24: Borrego Mtn seismic wave.

Table 8: Maximum displacement of the structure under the action of seismic waves in the *X* direction.

Seismic wave	The wooden frame is not reinforced with wooden pins (mm)			The wooden frame is reinforced with wooden pins (mm)		
	X	*Y*	*Z*	*X*	*Y*	*Z*
Parkfield	5.1600	0.4748	1.381	5.160	0.5824	0.6852
Borrego Mtn	5.5570	0.4594	1.191	3.829	0.1845	0.4979
Artificial waves	10.05	0.8222	1.281	8.686	0.7413	0.9965

Table 9: Maximum displacement of the structure under the action of seismic waves in the *Y* direction.

Seismic wave	The wooden frame is not reinforced with wooden pins (mm)			The wooden frame is reinforced with wooden pins (mm)		
	X	*Y*	*Z*	*X*	*Y*	*Z*
Parkfield	10.05	0.8222	1.281	0.1979	5.169	0.6467
Borrego Mtn	0.03825	5.120	1.103	0.1394	4.520	0.4447
Artificial waves	10.05	0.8222	1.281	0.2932	9.538	1.599

Table 10: Maximum displacement of the structure under the action of bidirectional horizontal seismic waves.

Seismic wave	The wooden frame is not reinforced with wooden pins (mm)			The wooden frame is reinforced with wooden pins (mm)		
	X	Y	Z	X	Y	Z
Parkfield	5.160	4.386	1.449	5.160	4.386	1.443
Borrego Mtn	5.552	3.966	1.354	5.408	4.056	1.389
Artificial waves	10.13	7.930	1.408	10.16	8.462	1.484

Table 11: Structural displacement under seismic waves in the X direction.

Seismic wave	The wooden frame is not reinforced with wooden pins (mm)				The wooden frame is reinforced with wooden pins (mm)			
	Outer column	Inner column	Middle layer column	Top column	Outer column	Inner column	Middle layer column	Top column
Parkfield	-3.710	-1.286	1.351	-2.216	-1.419	-2.49	0.578	-1.4192
Borrego Mtn	5.556	-1.119	1.064	1.083	3.829	-0.834	0.326	-0.625
Artificial waves	9.307	-1.719	1.187	1.502	7.593	1.183	0.368	1.586

Where the "-" sign represents the opposite direction to the assumed.

Table 12: Structural displacement under seismic waves in the Y direction.

Seismic wave	The wooden frame is not reinforced with wooden pins (mm)				The wooden frame is reinforced with wooden pins (mm)			
	Outer column	Inner column	Middle layer column	Top column	Outer column	Inner column	Middle layer column	Top column
Parkfield	9.307	-1.719	1.187	1.502	-5.089	-3.515	-3.098	-2.901
Borrego Mtn	4.033	-0.430	1.003	1.125	3.554	0.158	0.336	0.307
Artificial waves	9.307	-1.719	1.187	1.502	7.074	1.731	1.387	1.379

Where the "-" sign represents the opposite direction to the assumed.

Table 13: Structural displacement under the bidirectional horizontal seismic waves.

Seismic wave	The wooden frame is not reinforced with wooden pins (mm)				The wooden frame is reinforced with wooden pins (mm)			
	Outer column	Inner column	Middle layer column	Top column	Outer column	Inner column	Middle layer column	Top column
Parkfield	-3.978	-3.336	-3.177	-3.106	-4.080	-3.366	-3.294	-3.203
Borrego Mtn	5.525	-1.121	1.088	1.098	5.408	-1.225	1.129	1.124
Artificial waves	9.242	1.736	1.208	1.570	9.157	1.683	1.064	1.975

Where the "-" sign represents the opposite direction to the assumed.

gold Zhu, and Melon pillar top are extracted for analysis (Tables 11–13).

The displacement at the outer column is largest than in the other places. The displacement of the inner column is less than the middle layer column. The displacement of the top column is different in different types of seismic waves. The deformation between the different parts of structures is not coordinated under the action of earthquakes, which leads to torsional deformation. The reinforced inner column and middle layer column by wood pins are better than the top column. The stability of the inner column can be increased by the reinforcement of the penetration beam and first layer beam.

The displacement response of the vertices of each column is different under different seismic waves. However, the changing trend remains consistent. The displacement of the outer column and the inner column of the structure is quite different. Under the action of the same seismic wave. It can be judged that the main weak part of the seismic performance of the wood structure is located on the outer column. The displacement of the outer column and the inner column reinforced by the wooden pin is decreased compared to the outer column and the inner column without reinforcement, indicating that the reinforcement of the wooden pin enhances the seismic performance of the wood structure.

5. Conclusions

To better promote and inherit seismic reinforcement for the wooden structure, this paper is conducting large number of field research, consulting relevant technical personnel, and consulting relevant materials to learn more about the form of MTJ and structural characteristics of the wooden structure. Combined with the experimental data, it is found that ABAQUS can accurately simulate different forms of failure, such as wood fiber tearing and MTJ breaking. The bearing capacity of MJT reinforced with wooden pins is approximately 11.3% higher compared to that of MTJ without reinforcement. The displacement response of the single timber frame is mainly concentrated at the top of the structure by modes analysis. The frequency of the wooden truss is increased after reinforcement that is about 3%. Moreover, the wooden truss reinforced has changed in the 4th-order mode shape compared with the single wooden truss without reinforcement, which shows the reinforcement of wooden pins can significantly reduce the probability of deformation of the structure and increase the stiffness of the structure.

The reinforcement of wood pins effectively controls the horizontal displacement of the overall structure of the wooden frame, which is reduced by about 50%–62% compared with the unreinforced wooden frame. The larger displacement of the structure is concentrated on the second-layer beams and third-layer beams. Moreover, the result indicates the MTJ reinforced by the wooden pins that located on the upper layer of the structure has the better reinforcement effect on the timber frame. The reinforced inner column and middle layer column by wood pins are better than the top column. The stability of the inner column can be increased by the reinforcement of the penetration beam and first layer beam.

The optimal distribution of MTJ reinforced by wooden pins in the single wooden frame can improve the seismic performs of the single wooden frame. However, the optimal location of the MTJ reinforced by wooden pins in the whole wood frame still needs to be further investigated for improve the seismic performs of the traditional ancient wooden buildings.

Data Availability

The (DATA TYPE) data used to support the findings of this study are included within the article.

Disclosure

The authors alone are responsible for the content and writing of this article.

Conflicts of Interest

We declare that we have no financial and personal relationships with other people or organizations that can inappropriately influence our work. There is no professional or other personal interest of any nature or kind in any product, service, and/or company that could be construed as influencing the position presented in, or the review of, the manuscript entitled. The authors report no conflicts of interest.

Authors' Contributions

Hua Zhang and Wuping Gao contributed in the methodology. Wuping Gao contributed in the idea, supervision, and writing–original draft. Hua Zhang and Yanling Wang contributed in the writing–review and editing, discussion, and validation. The authors writing and review the manuscript revision and the final draft for important intellectual content.

Acknowledgments

This work was financially supported by the China Science and Nature Foundation (41772123), Spark Program of Earthquake Sciences (XH23004YA), and Technical Innovation, Inheritance and Promotion of Reed Painting Art in Xiongan New Area (HB20-YB111).

References

[1] S. Li, Z. Jiang, H. Luo, and L. Zhang, "Seismic behaviour of straight-tenon wood frames with column foot damage," *Advances in Civil Engineering*, vol. 2019, Article ID 1604208, 10 pages, 2019.

[2] R.-Y. Yang, Y.-F. Sun, and X.-F. Zhang, "Application and progress of reinforcement technology for Chinese ancient buildings with wood structure," *Geotechnical and Geological Engineering*, vol. 38, no. 6, pp. 5695–5701, 2020.

[3] S. C. Liang, *A Pictorial History of Chinese Architecture: A Study of the Development of Its Structural System and the Evolution of Its Types*, MIT Press, Cambridge, MA, USA, 1984.

[4] W. Bai, M. A. Moustafa, J. Dai, Y. Yang, K. Du, and X. Chen, "Damage assessment of Shuanghe Confucian temple after Changning earthquake mainshock and aftershocks series," *Bulletin of Earthquake Engineering*, vol. 19, no. 14, pp. 5977–6001, 2021.

[5] C. Liu, D. Fang, and L. Zhao, "Reflection on earthquake damage of buildings in 2015 Nepal earthquake and seismic measures for post-earthquake reconstruction," *Structures*, vol. 30, pp. 647–658, 2021.

[6] C. Bertolini Cestari and T. Marzi, "Conservation of historic timber roof structures of Italian architectural heritage: diagnosis, assessment, and intervention," *International Journal of Architectural Heritage*, vol. 12, no. 4, pp. 632–665, 2018.

[7] H. Huang, Y. Wu, Z. Li, Z. Sun, and Z. Chen, "Seismic behavior of Chuan-Dou type timber frames," *Engineering Structures*, vol. 167, pp. 725–739, 2018.

[8] X. Sun, X. Tao, S. Duan, and C. Liu, "Kappa (k) derived from accelerograms recorded in the 2008 Wenchuan mainshock, Sichuan, China," *Journal of Asian Earth Sciences*, vol. 73, no. 2013, pp. 306–316, 2013.

[9] K.-U. Schober, A. M. Harte, R. Kliger, R. Jockwer, Q. Xu, and J.-F. Chen, "FRP reinforcement of timber structures," *Construction and Building Materials*, vol. 97, pp. 106–118, 2015.

[10] M. A. Hassan, M. Usman, A. Hanif, S. H. Farooq, and J. Ahmed, "Improving structural performance of timber wall panels by inexpensive FRP retrofitting techniques," *Journal of Building Engineering*, vol. 27, Article ID 101004, 2020.

[11] M. Corradi, C. Mouli Vemury, V. Edmondson, K. Poologanathan, and B. Nagaratnam, "Local FRP reinforcement of existing timber beams," *Composite Structures*, vol. 258, p. 113363, 2021.
[12] M. Corradi, T. P. Vo, K. Poologanathan, and A. I. Osofero, "Flexural behaviour of hardwood and softwood beams with mechanically connected GFRP plates," *Composite Structures*, vol. 206, no. 206, pp. 610–620, 2018.
[13] H. Hoseinpour, M. R. Valluzzi, E. Garbin, and M. Panizza, "Analytical investigation of timber beams strengthened with composite materials," *Construction and Building Materials*, vol. 191, pp. 1242–1251, 2018.
[14] R. Steiger, E. Serrano, M. Stepinac et al., "Strengthening of timber structures with glued-in rods," *Construction and Building Materials*, vol. 97, no. 97, pp. 90–105, 2015.
[15] M. Branco, A. Gonçalves, L. Guerreiro, and J. Ferreira, "Cyclic behavior of composite timber-masonry wall in quasi-dynamic conditions reinforced with superelastic damper," *Construction and Building Materials*, vol. 52, no. 52, pp. 166–176, 2014.
[16] J. Xue, C. Wu, X. Zhang, and Z. Qi, "Experimental and numerical study of mortise–tenon joints reinforced with innovative friction damper," *Engineering Structures*, vol. 230, Article ID 111701, 2021.
[17] J. Xue, C. Wu, X. Zhang, and Y. Zhang, "Experimental study on seismic behavior of mortise–tenon joints reinforced with shape memory alloy," *Engineering Structures*, vol. 218, Article ID 110839, 2020.
[18] M. Izzi and A. Polastri, "Low cycle ductile performance of screws used in timber structures," *Construction and Building Materials*, vol. 217, pp. 416–426, 2019.
[19] G. Schiro, I. Giongo, W. Sebastian, D. Riccadonna, and M. Piazza, "Testing of timber-to-timber screw-connections in hybrid configurations," *Construction and Building Materials*, vol. 171, pp. 170–186, 2018.
[20] C. Zhang, H. Guo, K. Jung, R. Harris, and W.-S. Chang, "Screw reinforcement on dowel-type moment-resisting connections with cracks," *Construction and Building Materials*, vol. 215, no. 215, pp. 59–72, 2019.
[21] X. Song, K. Li, E. Crayssac, and Y. Wu, "Lateral performance of traditional heavy timber frames with mortise–tenon joints retrofitted using self-tapping screws," *Journal of Structural Engineering*, vol. 144, no. 10, Article ID 04018187, 2018.
[22] Y. J. Kim, M. Hossain, and K. A. Harries, "CFRP strengthening of timber beams recovered from a 32 year old quonset: element and system level tests," *Engineering Structures*, vol. 57, pp. 213–221, 2013.
[23] R. Jockwer, G. Fink, and J. Köhler, "Assessment of the failure behaviour and reliability of timber connections with multiple dowel-type fasteners," *Engineering Structures*, vol. 172, pp. 76–84, 2018.
[24] J. Jasieńko and T. P. Nowak, "Solid timber beams strengthened with steel plates—experimental studies," *Construction and Building Materials*, vol. 63, pp. 81–88, 2014.
[25] M. Verbist, J. M. Branco, E. Poletti, T. Descamps, and P. B. Lourenco, "Experimentations on the retrofitting of damaged single step joints with self-tapping screws," *Materials and Structures*, vol. 51, no. 4, Article ID 106, 2018.
[26] Q. Xie, L. Zhang, Z. Miao, W. Zhou, and S. Li, "Lateral behavior of traditional chinese timber-frames strengthened with shape-memory alloy: experiments and analytical model," *Journal of Structural Engineering*, vol. 146, no. 6, Article ID 04020083, 2020.
[27] J. M. Branco, M. Piazza, and P. J. S. Cruz, "Experimental evaluation of different strengthening techniques of traditional timber connections," *Engineering Structures*, vol. 33, no. 8, pp. 2259–2270, 2011.
[28] A. Shabani, A. Alinejad, M. Teymouri, A. N. Costa, M. Shabani, and M. Kioumarsi, "Seismic vulnerability assessment and strengthening of heritage timber buildings: a review," *Buildings*, vol. 11, no. 12, Article ID 661, 2021.
[29] M. B. Bağbancı and Ö. K. Bağbancı, "The dynamic properties of historic timber-framed masonry structures in Bursa, Turkey," *Shock and Vibration*, vol. 2018, Article ID 3257434, 11 pages, 2018.
[30] D. P. Fang, S. Iwasaki, M. H. Yu, Q. P. Shen, Y. Miyamoto, and H. Hikosaka, "Ancient Chinese timber architecture. II: dynamic characteristics," *Journal of Structural Engineering*, vol. 127, no. 11, pp. 1358–1364, 2001.
[31] C. Chen, H. Qiu, and Y. Lu, "Flexural behaviour of timber dovetail mortise–tenon joints," *Construction and Building Materials*, vol. 112, pp. 366–377, 2016.
[32] J. H. Zhao, M. H. Yu, D. F. Gao, and J. B. Sun, "FEM analysis on the elasto-plasticity of ancient wooden structure," *Journal of Xi'an University of Architecture & Technology (Natural Science Edition)*, vol. 31, no. 2, pp. 131–133, 1999.
[33] Y. P. Dong, R. X. Zhai, M. H. Yu, and R. L. Yu, "Reasons for northward descent Ofbaoguo temple hall in Ningbo," *Sciences of Conservation and Archaeology*, vol. 15, no. 4, pp. 1–5, 2003.
[34] Z. W. Guan, A. Kitamori, and K. Komatsu, "Experimental study and finite element modelling of Japanese "Nuki" joints—Part two: Racking resistance subjected to different wedge configurations," *Engineering Structures*, vol. 30, no. 7, pp. 2041–2049, 2008.
[35] J. Wang, J. He, N. Yang, and Q. Yang, "Study on aseismic characteristics of Tibetan ancient timber structure," *Advances in Materials Science and Engineering*, vol. 2017, Article ID 8186768, 15 pages, 2017.
[36] S. C. Liang, "Qinggong Ministry "Code of Engineering Practice"," Tsinghua University Press, 2006.
[37] J. Li, *Yingzao Fashi Construction Method*, Royal Press, Kaifeng, China, (in ancient Chinese), 1103.
[38] W. Q. Wang, "Engineering practice rules of the Qing Ministry of Public Works," *Engineering Construction Standardization*, vol. 2000, no. 2, Article ID 43, 2000.
[39] B. J. Ma, "Ancient Chinese building wood construction technology," Science Press, Bejing, 2003.
[40] J. Wang, J. X. He, Q. S. Yang, and N. Yang, "Study on mechanical behaviors of column foot joint in traditional timber structure," *Structural Engineering and Mechanics*, vol. 66, no. 1, pp. 1–14, 2018.
[41] S.-F. Jiang, M.-H. Wu, S.-L. Ma, and D.-Y. Lin, "Structural stiffness identification of traditional mortise–tenon joints based on statistical process control chart," *Journal of Aerospace Engineering*, vol. 31, no. 5, Article ID 04018066, 2018.
[42] S.-C. Li, L.-K. Chen, L.-Z. Jiang, and J.-Q. Li, "Experimental investigation on the seismic behavior of the semi-rigid one-way straight mortise–tenon joint of a historical timber building," *International Journal of Architectural Heritage*, vol. 14, no. 8, pp. 1135–1147, 2020.
[43] C. C. Chen, H. X. Qiu, and M. G. Xu, "Experimental study on flexural behavior of typical mortise–tenon joints," *Applied Mechanics and Materials*, vol. 578-579, pp. 160–163, 2014.
[44] L.-K. Chen, S.-C. Li, Y.-T. Wang et al., "Experimental study on the seismic behaviour of mortise–tenon joints of the ancient timbers," *Structural Engineering International*, vol. 27, no. 4, pp. 512–519, 2018.

[45] Z. Y. Chen, "Behaviour of typical joints and the structure of Yingxian Wood Pagoda," Harbin Institute of Technology, Harbin, China, Doctoral Dissertation, 2010.
[46] Q. Chun, Z. Yue, and J. W. Pan, "Experimental study on seismic characteristics of typical mortise–tenon joints of Chinese southern traditional timber frame buildings," *Science China Technological Sciences*, vol. 54, no. 9, pp. 2404–2411, 2011.
[47] P. Obara, "Verification of orthotropic model of wood," *Archives of Civil Engineering*, vol. LXIV, no. 3, 2018, 2018.
[48] Y. Pan, R. B. An, X. Y. Wang, and R. Guo, "Study on mechanical model of through-tenon joints in ancient timber structures," *China Civil Engineering Journal*, vol. 53, no. 4, pp. 61–70+82, 2020.
[49] J. Y. Xue, P. Lu, and H. L. Xia, "Analysis of influencing factors of force performance of permeable joints of ancient building wood structure," *Journal of Xi'an University of Architecture and Technology (Natural Science Edition)*, vol. 50, no. 3, pp. 324–330, 2018.
[50] Y. L. Gao, "Experimental study and theoretical analysis of typical mortise and tenon joints of traditional wood structures based on wood friction mechanism and embedded pressing characteristics," Kunming University of Science and Technology, Kunming, China, 2017.
[51] E. Crayssac, X. Song, Y. Wu, and K. Li, "Lateral performance of mortise–tenon jointed traditional timber frames with wood panel infill," *Engineering Structures*, vol. 161, pp. 223–230, 2018.
[52] GB 50011-2010, *Code for Seismic Design of Buildings*, China Architecture & Building Press, Beijing, 2010.